Optimization of tungsten oxide films electro-deposited on macroporous silicon for gas sensing applications: Effect of annealing temperature

N. Mendoza-Agüero, Y. Kumar, S.F. Olive-Méndez, J. Campos-Alvarez, V. Agarwal.

Abstract

Polycrystalline WO_3 films grown on macroporous silicon via electrochemical deposition, have been studied as a function of annealing temperature. The hybrid structure was characterized using scanning electron microscopy, energy-dispersive X-ray spectroscopy, X-ray diffraction and Fourier transform infrared spectroscopy. The microstructure and grain-size of the metal oxide film were found to have significant influence on its electrical and sensing properties. DC conductivity measurements reveal the rectifying behavior of the junction, which is found to increase with annealing temperature. The increased sensitivity of the samples annealed at 700 °C has been attributed to a lower grain size, which contributes to an increase in the depletion region per unit length. An extrapolation of the variation of the resistance $\Delta R/R_0 = 1.5$ % predicts possible ethanol sensing up to 1 ppm.

Introduction

Transition metallic oxides have attracted attention as sensor materials due to their sensitivity towards different kinds of gases [1–4]. Among the different metal oxides, tungsten oxide (WO_x; this nomenclature is used due to fact that tungsten oxide is a sub-stoichiometric material) is very popular due to its wide band gap and is found to be very useful in areas such as sensing, catalysis, electrochemical industry and field emitters

[5–7]. Apart from this, WO_x possesses electrochromic, optochromic and gasochromic properties [8], which have been applied to design smart windows, electrochromic displays, etc. [9]. In the recent past, scientific community is aggressively looking for cheap, reliable and high-performance sensors for monitoring different gases. Tungsten oxide is an important semiconductor and is considered as one of the most promising materials for sensing applications. Furthermore, this semiconducting material can be fabricated in thin films to optimize its properties, i.e., to minimize the size of the devices and to integrate with the silicon technology [10].

WO_x thin films can be prepared by various techniques [11–14] and under different processing conditions, the films usually possess different microstructures and properties. In the recent years, tungsten oxide 1D nanostructures have been mainly grown on silicon or tungsten substrates [15]. Different types of porous substrates have also been used for improving the sensing response of WO_x, e.g. porous alumina [16] or macroporous silicon (MPS) [17].

In particular porous silicon (PS) has various interesting properties for sensing applications, such as variable surface chemistry and high chemical reactivity [18,19]. Apart from these properties, it has open structure (pores) and large surface area. In general, the versatile nature of PS makes it an ideal substrate for potential applications in the field of optoelectronics, photovoltaics, gas sensors, photonics and biomedical applications [20–24].

Several studies of WO_x deposited on silicon have been reported, e.g. Fang et al. [25] reported WO_x films with different stoichiometries, deposited on Si(111) wafers by pulsed laser deposition technique; Galléa et al. [26] investigated the growth process of

WO_x nanostructures deposited on Si substrates by a thermal oxidation and constructed a phase growth diagram with the possibility to realize the phase selection and morphology control of WO_x. Recently Yan et al. [27] synthesized WO_x nanoparticles by sol–gel method and deposited it onto the porous silicon and alumina substrates by dip-coating. Gas sensing tests experimentally demonstrated an improved NO_2-sensing with PS substrates decorated with WO_3 nanoparticles, as compared to WOx deposited on alumina or pristine/pure PS. The same group [28] prepared n-WO_{3-x}/n-PS junctions (by sputtering) for NO_2 sensing. The sensor exhibited a strong response, fast response/recovery rate, excellent repeatability and good selectivity for efficient detection of NO_2 at ppb level. Finally, our group [29] has recently studied optical and structural properties of WO_x electrodeposited on luminescent meso-porous silicon resulting in an increase of photoluminescence intensity with annealing temperature under nitrogen atmosphere in contrast with air atmosphere.

Ma et al. [15,16,28] have grown different morphologies of tungsten oxide onto MPS for gas sensing application using an expensive, complex and time consuming technique for such deposition [27]. In the present work, optical, structural, electrical and sensing properties of WO_x films, deposited onto the MPS substrate through inexpensive, facile and rapid technique (i.e. electrodeposition), have been studied as the function of annealing temperature.

Experimental

Preparation of porous silicon: MPS was formed by an electrochemical etching of (100)-oriented, boron-doped p-type silicon substrates of resistivity 14–22 Ω cm, using an electrolyte consisting of 4 wt% hydrofluoric acid (48 wt%) in N'N-Dimethylformamide

(ACS reagent, ≥99.8%). The current density during anodization was kept at 6 mA/cm^2 for 1 h. After fabrication, the samples were rinsed with N'N-Dimethylformamide (DMF) and dried with slow nitrogen flux.

Electrodeposition of WO_x: Thin films of WO_x were obtained by electrodeposition in a peroxytungstic acid solution contained in an electrochemical cell with a platinum mesh as the auxiliary electrode and MPS as the working electrode. The working electrode was subjected to a constant cathodic potential of 10 V with different deposition time of 20 and 30 min. The obtained WO_x films were homogenous, stable and transparent. Effect of heat treatment on the hybrid structures was studied at 500 and 700 °C for one hour under air atmosphere.

Structural properties of MPS and its composite with WO_x were analyzed using a scanning electron microscope (SEM) Hitachi VP-SEM SU1510. The orientation and crystallinity of WO_x was analyzed by XRD (Xpert'PRO) using CuKα radiation having wavelength of 1.54 Å. Fourier Transform Infrared spectroscopy (FTIR) model Cary 660 was used for obtaining the information about the chemical bonds formed in the composite structure. The transport characteristics were studied with the help of DC resistance measurements through the lateral and transverse configuration. The gas sensing measurements were carried out in homemade static gas sensing characterization system with the ability to control the ethanol concentration through mass fluxmeters. PPM concentration in the chamber was calculated by the pressure variation using a pirani gauge. To confirm the presence of oxygen vacancies, tungsten oxide powder from Sigma Aldrich of 99.9% purity was used as a reference.

Results and discussion

Fig. 1 shows top and cross-sectional SEM micrographs of as prepared MPS. These images reveal a uniform surface and squared/rounded shape pores of ~1 μm diameter (see inset in Fig. 1a). The corresponding cross-sectional images showing the macroporous structure of the PS layer is shown in Fig. 1b. The silicon wafers were etched for 60 min for the formation of ~28 μm thick porous layer.

Fig. 2 shows the top and cross-sectional SEM images of some hybrid structures (MPS–WO_x). It is a granular structure distributed all around the pore walls. Magnified view is shown as inset in Fig. 2c. An increase in the deposition time from 20 to 30 min resulted in the formation of some agglomerates on the porous surface as well. The presence of WO_x throughout the pore depth was confirmed by energy-dispersive X-ray spectroscopy (EDS) analysis given in the latter part of the manuscript.

Fig. 3 shows the top and cross-section view of WO_x–MPS composites after annealing at 500 and 700 °C respectively for 1 h under air atmosphere. WO_x is found to cover the pore walls and the adhesion of WO_x along the pore depth in the form of thin film is a common feature at both the annealing temperatures. Other notable difference observed at 700 °C is the accumulation of WO_x at the bottom of pore (encircled in Fig. 3d). Formation of WO_x agglomerates at the bottom of the pores at 700 °C possibly results in the thin WO_x layer left on the pore walls.

FTIR is a technique used to obtain information about the chemical bonding in a material. The FTIR spectra taken through an attenuated total reflectance (ATR) accessory of as-deposited and annealed WO_x–MPS hybrid structures are shown in Fig. 4. The spectra of as-deposited WO_x films (Fig. 4a) reveal absorption bands at 541 and 560 cm^{-1}. Such values are slightly shifted compared to the bands at 550 and 572 cm^{-1},

which have been shown in WO_3 films fabricated by the sol–gel technique and correspond to the peroxo groups W–O–O stretch modes [30]. Fig. 4a also presents a band at 608 cm^{-1}, which is displaced from 612 cm^{-1} and can be assigned to the O–W–O stretch, typical of crystalline hydrated oxides of tungsten [31].

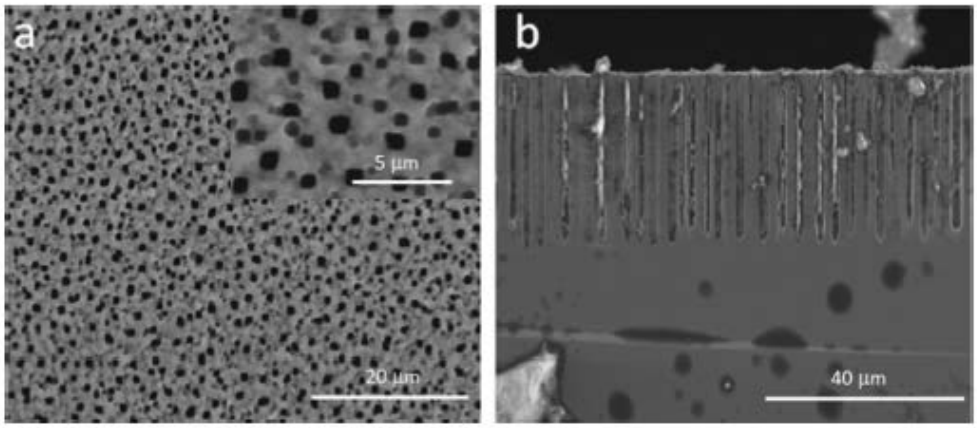

Fig. 1. SEM images of MPS: (a) Top view and (b) cross-section.

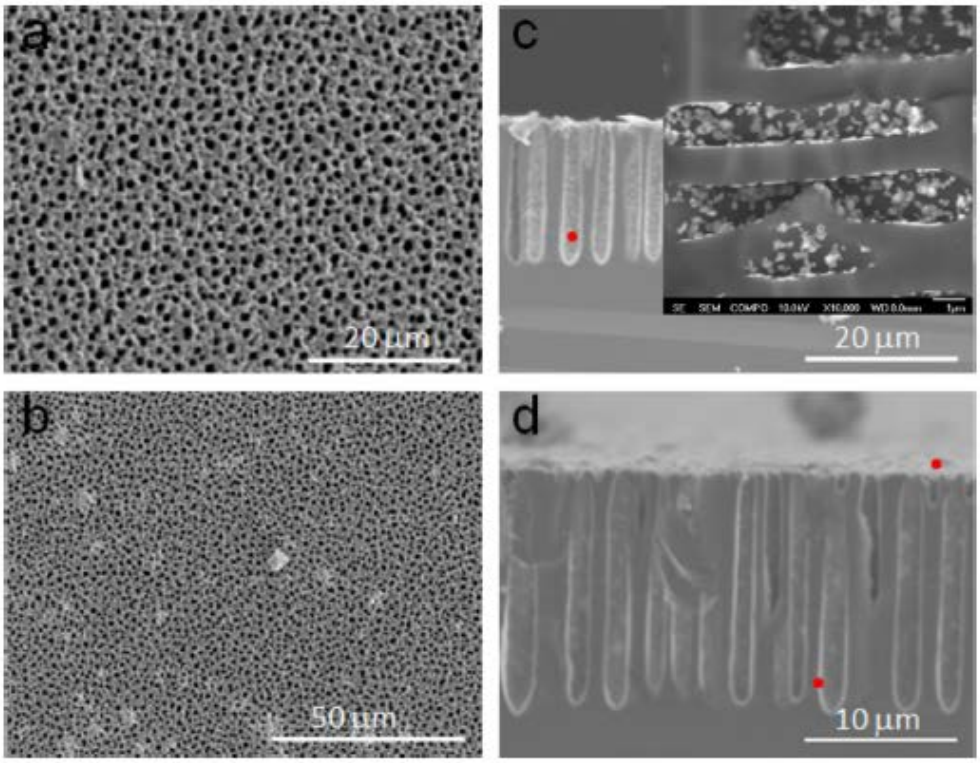

Fig. 2. SEM images of WO_x on macroporous silicon with different electrodeposition time. Top view: (a) 20 min, (b) 30 min and the corresponding cross-sections (c) 20 min and (d) 30 min. Magnified view of WO_x deposition shown as inset in Fig. 2c.

This observation suggests the presence of crystalline portion in WO_x matrix without annealing treatment. Well-defined bands seen at 733 and 892 cm^{-1}, in the spectrum of the sample annealed at 500 1C (Fig. 4b) have been attributed to W–O groups and O–W–O inter-bridging stretching mode respectively [32], taken from IR data on sol–gel-derived WO_x films obtained from a peroxytungstate sol. The absence of a band at 560 cm^{-1} indicates the absence of W–O–O groups due to the annealing effect, which condenses the WOx molecular structure. On the other hand, intensity band at 610 cm^{-1} increases suggesting the presence of more crystalline WO_x compound.

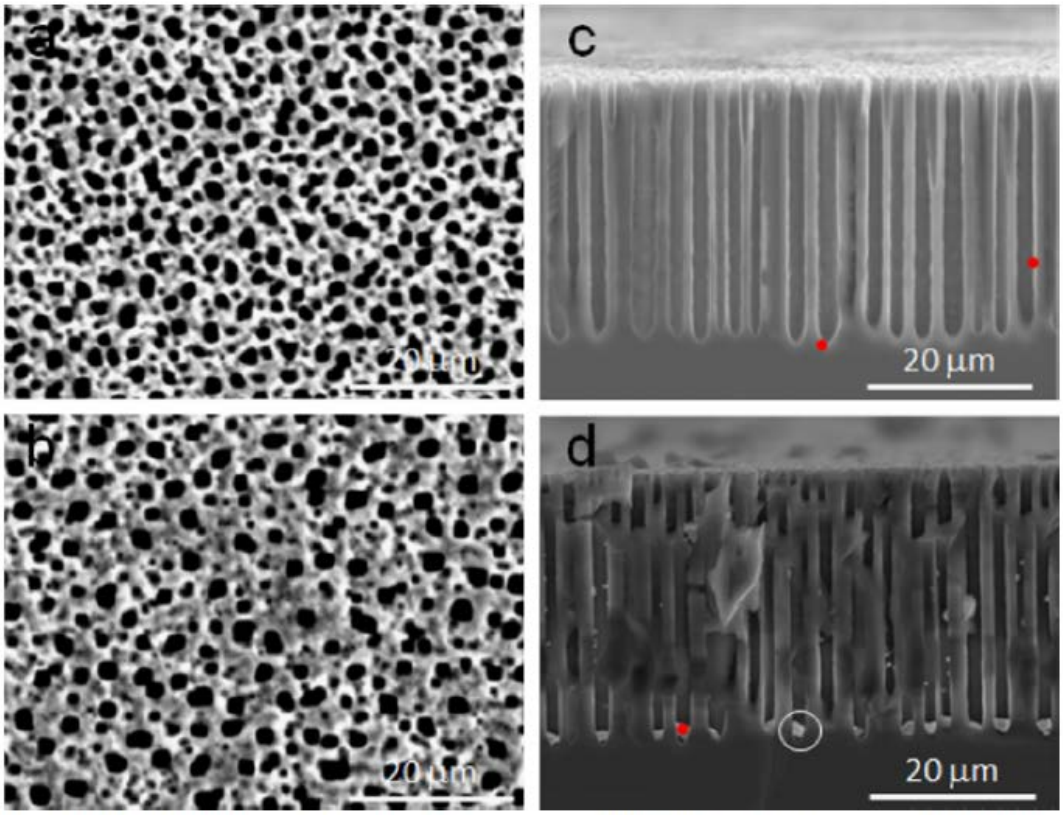

Fig. 3. SEM images of WO_x–MPS hybrid structures at different annealing temperatures (a) 500 and (b) 700 °C. Circled part is an example of WO_x aggregates at the bottom of the macroporous silicon matrix.

Further annealing at 700 °C generates the presence of a new band at 809 cm^{-1} as a shoulder which arises from the (W–O–W) bridging stretch [33,34], while bands at

905 and 952 cm^{-1} can be attributed to the symmetric stretching vibrational mode of terminal W=O bonds located on the surface of the WO_x clusters [35,36]. Moreover, an increase in the intensity of the band at 610 cm^{-1} indicates an enhancement in the crystallinity of WO_x nanostructures.

Fig. 5 shows the XRD analysis to understand the crystalline nature of the WO_x–MPS composites after annealing at 700 °C (Fig. 5a) and 500 °C (Fig. 5b). XRD patterns of WO_x films display a polycrystalline nature. The presence of sharp peaks at angles 2θ=23.1°, 23.7°, 24.4° for annealed sample at 500 °C (Fig. 5b) represent the monoclinic phase of (002), (020), (200) planes [37], repectively. In addition 2θ=51.51 correspond to the tetragonal phase [38,39]; thus this structure presents both types of crystalline phases. It is also evident that the intensity of the peaks, at 23.1° and 23.7° disappears after annealing at 700 °C. It is attributed to the fact that the measurements are being carried out at a grazing angle of 0.5° and after annealing at higher temperature most of WO_x crystals have agglomerated at the bottom of the pore, leaving a very thin film of WO_x on the pore walls. Additionally, the shifting of two peaks at 24.4° and 51.5° to 25.0° and 52.6° suggests induced stress on the films at higher annealing temperature. The peak at 2θ=55.8° corresponds to PS which is present in both samples. Furthermore, the grain size from XRD data has been estimated by means of Scherrer's formula. The observed XRD pattern and other details are summarized in Table 1.

The current–voltage (I–V) curves of MPS and WO_x–MPS (Fig. 6), measured at a sweep rate of 50 mV/s, for the reference sample and both the annealing temperatures. The I–V curve of the reference MPS sample demonstrates a Schottky contact between Ag and MPS layer. The annealed samples demonstrate a non-ohmic electrical response

in a sandwich configuration (inset of Fig. 6). Such behavior is attributed to the formation of Schottky barriers at the WO_x–MPS interfaces. ±–V plot, displayed as inset, corresponds to a zoom between 71 V to show the relative difference between the diode-like behavior of the hybrid structures. Samples annealed at 700 °C present higher forward/reverse current compared to those annealed at 500 °C. Hybrid structures annealed at 700 °C present lesser resistance, possibly due to the relative decrease in the presence of insulating oxides on the surface along with the type of crystalline phase (formed) in each annealing process, i.e. a mixture of monoclinic-tetragonal phase present at 500 °C and tetragonal at 700 °C is possibly affecting the electrical behavior of the p–n junctions. In order to quantify the deviation from the Schottky behavior, the rectifying factor (I_F/I_R) was calculated at 1 V for both the samples and found to be about 0.04 and 0.13 for 500 and 700 °C respectively.

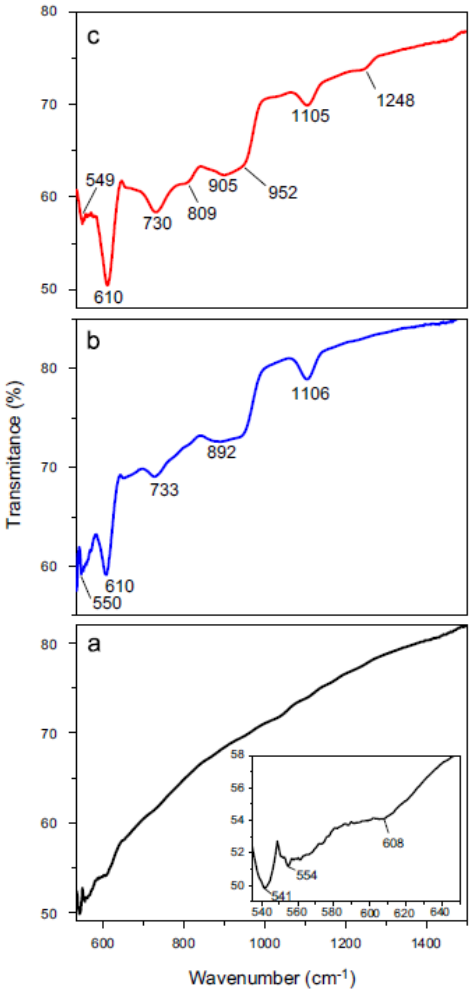

Fig. 4. FTIR transmittance spectra of: (a) as-deposited WO_x–MPS structures (b) annealed at 500 and (c) 700 °C. Samples were annealed for 1 h under normal atmospheric conditions. (Inset shows a magnified view).

In accordance with the obtained results, WO_x–PS structures annealed at 700 °C possess relatively higher rectifying factor, a required characteristic for electronic applications. Thus an optimization in the annealing process is found to be necessary to find the characteristic parameters for potential applications in diode technology.

Fig. 7(a) and (b) shows the sensing response (for ethanol vapors) of MPS–WO_x hybrid structures. Sample annealed at 500 °C detects ethanol at a concentration as low as 30 ppm with a variation of the resistivity $\Delta R/R_0$=1.5% and a recovery time of 40 s at

50 ppm. The decrease of resistance of the off states can be attributed to an inhomogeneous ethanol desorption, which, at the same time, can be attributed to a higher electronic affinity [40] dependent on the stoichiometry of the samples (W/O ratio).

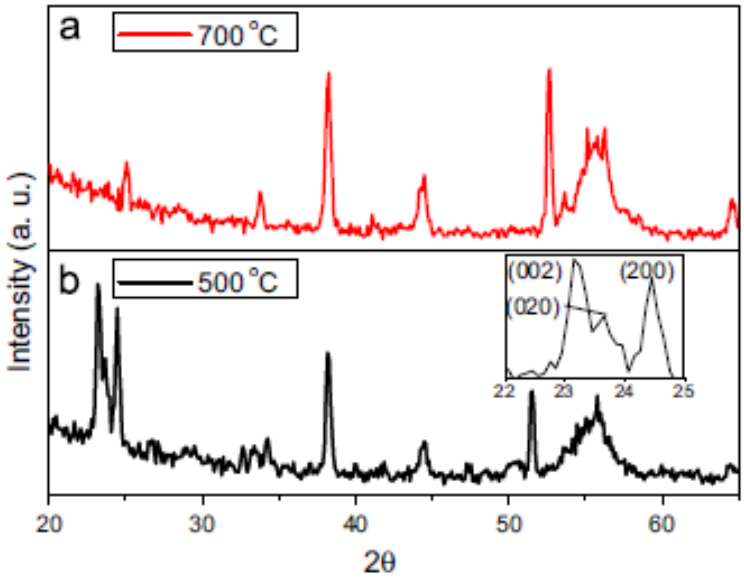

Fig. 5. XRD patterns of WO_x films electrodeposited on MPS substrate annealed at: (a) 500 and (b) 700 °C for 1 h under normal conditions.

Table 1
Average crystallite size determined using Scherrer's formula.

WO_3/PS Sample	Planes	2θ	FWHM	Size τ (nm)
500 °C	(002)	23.1	0.0045	31.4
	(020)	23.7	0.0043	32.2
	(200)	24.4	0.0052	27.2
700 °C	200	25.0	0.0075	18.9

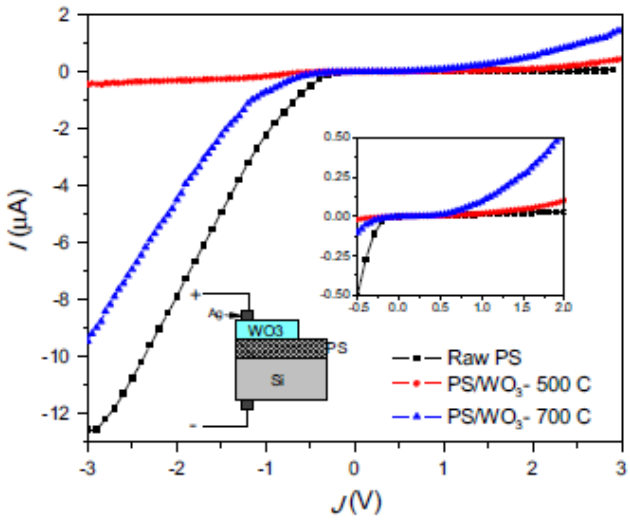

Fig. 6. Current–voltage (I–V) curves of reference MPS and WO_x–MPS heterostructures annealed at different temperatures.

For an ethanol concentration of 200 ppm, ΔR=0.4 kΩ for sample annealed at 500 °C and 3.5kΩ for sample annealed at 700 °C, indicating the potential of the second sample to detect lower ethanol concentrations. For sample annealed at 700 °C, a plot of $\Delta R/R_0$, (for the measured concentrations) involves the possibility of an extrapolation of the fitted line to find the corresponding ethanol concentration for $\Delta R/R_0$=1.5%, showing that the detection limit is 1 ppm.

Conductivity in semiconducting oxides depends on the charge carrier density and the width of the depleted region at the grain surface for a polycrystalline film. The difference in sensitivity between the samples annealed at 500 and 700 °C is related to the relative change of width of the depleted region between their grains. Annealing performed at different temperatures allows different grain size (as a change on the chemical potential Δμ) and different stoichiometry as it will later demonstrated in this paper through EDS results (Table 2).

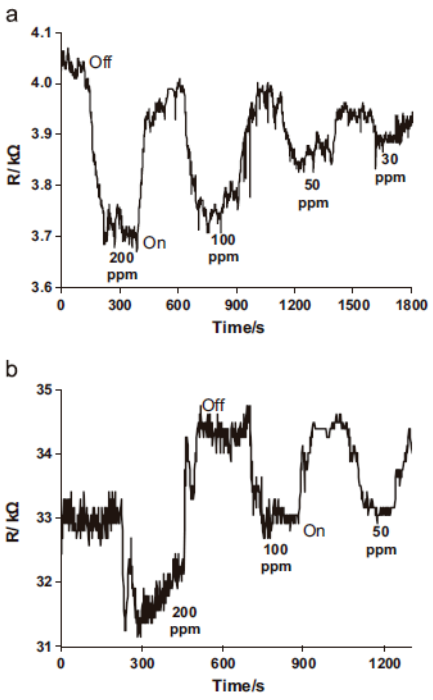

Fig. 7. Sensing characteristics performed at 300 °C for samples annealed at (a) 500 and (b) 700 °C. ΔR at 200 ppm are 0.4 and 3.5 kΩ for samples annealed at 500 and 700 °C, respectively. Sample annealed at 500 °C has a $\Delta R/R_0 = 1.5\%$ for an ethanol concentration of 30 ppm. Extrapolating $\Delta R/R_0$ for all measured concentrations for sample annealed at 700 °C reveals that for $\Delta R/R_0 = 1.5$ the sensibility limit is 1 ppm.

An excess of W would be reflected on the formation of oxygen vacancies (V_O), which are charge carrier donors (n-type semiconductor), hence the width of the potential barrier decreases with an increase in V_O concentration. Then the number of depleted regions that have to be traversed by conducting electrons, depends on the grain size, as the area of the sensing device for both samples is the same (4 mmx4 mm). Fig. 8 is the Arrhenius plot of R vs 1/T in order to evaluate the height of the potential barrier from the equation:

$$R = R_0 \exp^{\frac{eV_b}{kT}} \qquad (1)$$

where e is the electron charge, V_s is the height of the potential barrier, k is the Boltzmann constant and T is the absolute temperature. The slope of the fitted curve corresponds to the value $_eV_s$=k, then the depletion width can be calculated using

$$W = \lambda_D \sqrt{2eV_s/kT} \qquad (2)$$

where λD is the Debye length. Taking λ_D = 60 nm at 320 °C, from Ref. [41], this value is a good approximation for our sensing conditions performed at 300 °C. Solving Eq. (2), the depletion widths are 8 and 6 nm for samples annealed at 500 and 700 °C, respectively; this suggests that grains exclusively participating on the sensing characteristics from sample annealed at 700 °C, have greater concentration of V_O (charge carriers) than sample annealed at 500 °C, which are more near to the theoretical WO_3 stoichiometry, (less quantity of V_O). This relative enhancement in the concentration of charge carriers is also seen from I–V characteristics (Ref. to Fig. 6).

To confirm the presence of oxygen vacancies, EDS quantification was performed on PS–WO_x composite samples (results summarized in Table 2). The increase in the O/W ratio is attributed to the oxidation of silicon. In order to confirm the hypothesis additional samples were analyzed: a continuous WO_3 sputtered film on SiO_2/Si(001) substrate and pure WO_3 powders. Each sample was divided in three parts to evaluate W–O concentration without thermal treatment, and after annealing at 500 and 700 °C. Table 2 shows the Si/W and O/W ratios which demonstrate that on annealing, pure WO_3 powder looses a certain amount of oxygen atoms, i.e. formation of oxygen vacancies during thermal treatment. For WO_3/SiO_2/Si(001) films and WO_x/MPS composites the oxygen/tungsten ratio increases with annealing temperature. The

increase in oxygen content is attributed to silicon oxidation on both heterostructures, which in turn can be understood through higher Gibbs free energy of SiO_x (-856 kJ/mol) than that of WO_x (-764 kJ/mol); i.e., the formation of SiO_2 is an easier reaction than formation of WO_3. Hence an increase in the oxygen content can be attributed to silicon oxidation and at the same time oxygen vacancies are created in WO_3.

Conclusions

Formation of WO_3–macroporous silicon hybrid structures has been demonstrated via simple, fast and inexpensive technique i.e. electrochemical route. SEM images reveal the infiltration of WO_x into the macroporous matrix. The basic characterization of the hybrid structure shows a polycrystalline nature of the films with oxygen vacancies. XRD reveals two phases of WO_x at 500 °C, monoclinic and tetragonal, and only tetragonal phase in samples annealed at 700 °C. Temperature-dependent DC electrical conductivity of the polycrystalline WO_x films exhibits an exponential behavior, which indicates the semiconducting nature of all the films that can be exploited as a sensing device. Growth conditions and post-growth thermal treatment have a significant effect on the quality and stoichiometry of the films. For sample annealed at 500 °C a stoichiometry revealed the formation ofdepleted regions with a width of 8 nm, while sample annealed at 700 °C with higher charge carrier density the width is 6nm. Sample annealed at 700 °C was evaluated to be able to detect ethanol at a concentration up to 1 ppm.

Acknowledgment

Authors are thankful for financial support given by CONACyT project CB-128953. NM acknowledges PROMEP for the post doctoral fellowship.

References

[1] A. Afzal, N. Cioffi, L. Sabbatini, L. Torsi, NOx sensors based on semiconducting metal oxide nanostructures: progress and perspectives, Sens. Actuators B 171–172 (2012) 25–42.

[2] A. Lari, A. Khodadadi, Y. Mortazavi, Semiconducting metal oxides as electrode material for YSZ-based oxygen sensors, Sens. Actuators B 139 (2009) 361–368.

[3] B. Hu, W. Chen, J. Zhou, High performance flexible sensor based on inorganic nanomaterials, Sens. Actuators B 176 (2013) 522–533.

[4] H.J. Kim, J.H. Lee, Highly sensitive and selective gas sensors using p-type oxide semiconductors: overview, Sens. Actuators B 192 (2014) 607–627.

[5] M.U. Qadri, M.C. Pujol, J. Ferré-Borrull, E. Llobet, M. Aguiló, F. Díaz, WO3 thin films for optical gas sensing, Procedia Eng. 25 (2011) 260–263.

[6] X. Luo, F. Deng, L. Min, S. Luo, B. Guo, G. Zeng, C. Au, Facile onestep synthesis of inorganic-framework molecularly imprinted TiO2/WO3 nanocomposite and its molecular recognitive photocatalytic degradation of target contaminant, Environ. Sci. Technol. 47 (2013) 7404–7412.

[7] L. Meda, A.M. Dangerfield, M.C. Jones, C.M. White, A. Navulla, Electrochemical properties of tungsten oxide nanowires compared to bulk particles, Jpn. J. Appl. Phys. 51 (2012) 11PE06.

[8] D. Li, G. Wu, G. Gao, J. Shen, F. Huang, Ultrafast coloring-bleaching performance of nanoporous WO3–SiO2 gasochromic films doped with Pd catalyst, Appl. Mater. Interfaces 3 (2011) 4573–4579.

[9] J. Wang, X.W. Sun, Z. Jiao, Application of nanostructures in electrochromic materials and devices: recent progress, Materials 3 (2010) 5029–5053.

[10] M.J. Vellekoop, C.C.O. Visser, P.M. Sarro, A. Venema, Compatibility of zinc oxide with silicon IC processing, Sens. Actuators A: Phys. 23 (1990) 1027.

[11] N. Tahmasebi Garavand, M. Ranjbar, S.M. Mahdavi, A. Iraji Zad, , Colouration process of colloidal tungsten oxide nanoparticles in the presence of hydrogen gas, Appl. Surf. Sci. (2012) 10089–10094.

[12] Y.S. Kim, Thermal treatment effects on the material and gas-sensing properties of room-temperature tungsten oxide nanorod sensors, Sens. Actuators B 137 (2009) 297–304.

[13] T.A. Nguyen, S. Park, J.B. Kim, T.K. Kim, G.H. Seong, J. Choo, Y. S. Kim, Polycrystalline tungsten oxide nanofibers for gas-sensing applications, Sens. Actuators B 160 (2011) 549–554.

[14] Y. Zhang, J. Yuan, J. Le, L. Song, X. Hu, Structural and electrochromic properties of tungsten oxide prepared by surfactant-assisted process, Sol. Energy Mater. Sol. Cells 93 (2009) 1338–1344.

[15] S. Ma, M. Hun, P. Zeng, W. Yan, M. Li, Growth of tungsten oxide nanorods onto porous silicon and their sensing properties for NO2, Mater. Lett. 99 (2013) 57–60.

[16] M. Gillet, A. Al-Mohammad, C. Lemire, Microstructural analysis of WO3 thin films on alumina substrates, Thin Solid Films 410 (2002) 194–199.

[17] S. Ma, M. Hun, P. Zeng, M. Li, W. Yan, C. Li, Synthesis of tungsten oxide nanowires/porous silicon composites and their application in NO2 sensors, Mater. Lett. 112 (2013) 12–15.

[18] V. Torres-Costa, R.J. Martín-Palma, Application of nanostructured porous silicon in the field of optics. A review, J. Mater. Sci. 45 (2010) 2823–2838.

[19] R.C. Anderson, R.S. Muller, C.W. Tobias, Investigations of porous Si for

vapor sensing, Sens. Actuators A 21–23 (1990) 835–839.

[20] H. Foll, M. Christophersen, J. Carstensen, G. Hasse, Formation and application of porous silicon, Mater. Sci. Eng. R 39 (2002) 93–141.

[21] L. Pavesi, Z. Gaburro, L.D. Negro, P. Bettotti, G.V. Prakash, M. Cazzanelli, C.J. Oton, Nanostructured silicon as a photonic material, Opt. Lasers Eng. 39 (2003) 345–368.

[22] P. Granitzer, K. Rumpf, Porous silicon – a versatile host material, Materials 3 (2010) 943–998.

[23] E.J. Anglin, L. Cheng, W.R. Freeman, M.J. Sailor, Porous silicon in drug delivery devices and materials, Adv. Drug Deliv. Rev. 60 (2008) 1266–1277.

[24] P. Menna, G.D. Francia, V. La Ferrara, Porous silicon in solar cells: a review and description of its application as an AR coating, Sol. Energy Mater. Sol. Cells 37 (1995) 13–24.

[25] G. Fang, Z. Liu, K.L. Yao, Fabrication and characterization of electrochromic nanocrystalline WO3/Si (111) thin films for infrared emittance modulation applications, J. Phys. D: Appl. Phys. 34 (2001) 2260–2266.

[26] F. Galléa, Z. Li, Z. Zhang, Growth control of tungsten oxide nanostructures

on planar silicon substrates, Appl. Phys. Lett. 89 (2003) 193111.

[27] W. Yan, M. Hu, P. Zeng, S. Ma, M. Li, Room temperature NO2-sensing properties of WO3 nanoparticles/porous silicon, Appl. Surf. Sci. 292 (2014) 551–555.

[28] M. Li, M. Hu, D. Jia, S. Ma, W. Yan, NO2-sensing properties based on the nanocomposite of n-WO3"x/n-porous silicon at room temperature, Sens. Actuators B 186 (2013) 140–147.

[29] N. Mendoza-Agüero, V. Agarwal, Optical and structural characterization of tungsten oxide electrodeposited on nanostructured porous silicon: effect of annealing atmosphere and temperature, J. Alloys Compd. 581 (2013) 596–601.

[30] M. Deepa, P. Singh, S.N. Sharma, S.A. Agnihotry, Effect of humidity on structure and electrochromic properties of sol–gel-derived tungsten oxide films, Sol. Energy Mater. Sol. Cells 90 (2006) 2665–2682.

[31] M.F. Daniel, B. Desbat, J.C. Lassegues, B. Gerand, M. Figlarz, Infrared and Raman study of WO3 tungsten trioxides and WO3, xH2O tungsten trioxide hydrates, J. Solid State Chem. 67 (1987) 235.

[32] U.O. Krasovec, A.S. Vuk, B. Orel, IR Spectroscopic studies of charged–

discharged crystalline WO3 films, Electro Chim. Acta 46 (2001) 1921–1929.

[33] B. Orel, N. Groselj, U.O. Krasovec, R. Jese, A. Georg, IR spectroscopic investigations of gasochromic and electrochromic sol–gel-derived peroxotungstic acid/ormosil composite and crystalline WO3 films, J. Sol–Gel Sci. Technol. 24 (2002) 5–22.

[34] R. Solarska, B.D. Alexander, J. Augustynski, Electrochromic and photoelectrochemical characteristics of nanostructured WO3 films prepared by the sol–gel method, C.R. Chim. 9 (2006) 301–306.

[35] A. Kuzmin, J. Purans, E. Cazzanelli, C. Vinegoni, G. Mariotto, X-ray diffraction, extended X-ray absorption fine structure and Raman spectroscopy studies of WO3 powders and (1''x)WO3''yUxReO2 mixtures, J. Appl. Phys. 84 (1998) 5515.

[36] C. Santato, M. Odziemkopwski, M. Ulmann, J. Augustynski, Crystallographically oriented mesoporous WO3 films: synthesis, characterization, and applications, J. Am. Chem. Soc. 123 (2001) 10639–10649.

[37] A.H. Jayatissa, S.T. Cheng, Optoelectronic properties of nanocrystalline tungsten oxide thin films, IEEE-Nano (2002) 25–28 ISSN: 0169-555X, URL: !http://ieeexplore.ieee.org/xpl/articleDetails.jsp%3Freload%3Dtrue%

https://cimav.repositorioinstitucional.mx/jspui/

26arnumber%3D1032115%26contentType%3DConference%2BPublications".

[38] K. Bange, Colouration of tungsten oxide films: a model for optically active coatings, Sol. Energy Mater. Sol. Cells 58 (1999) 1–131.

[39] A. Al Mohammad, M. Gillet, Phase transformations in WO3 thin films during annealing, Thin Solid Films 408 (2002) 302–309.

[40] N. Barsan, U. Weimar, Conduction model of metal oxide gas sensors, J. Electroceram. 7 (2001) 143–167.

[41] A. Labidi, C. Lambert-Mauriat, C. Jacolin, M. Bendahan, M. Maaref, K. Aguir, DC and AC characterizations of WO3 sensors under ethanol vapors, Sens. Actuators B: Chem. 119 (2006) 374–379.